JOURNAL OF GEOPHYSICAL RESEARCH, VOL. 94, NO. B12, PAGES 17,497–17,510, DECEMBER 10, 1989

Tomographic Inversion of Local Earthquake Data From the Hengill-Grensdalur Central Volcano Complex, Iceland

D. R. TOOMEY

Department of Earth, Atmospheric, and Planetary Sciences, Massachusetts Institute of Technology, Cambridge

G. R. FOULGER

Department of Geological Sciences, University of Durham, Science Laboratories, Durham, England

We have determined the three-dimensional *P* wave velocity structure within the area of the Hengill-Grensdalur central volcano complex, southwest Iceland, from the tomographic inversion of 2409 *P* wave arrival times recorded by a local earthquake experiment. The aperture of the 20-element seismic network utilized in the inversion permitted imaging of a 5-km-thick crustal volume underlying a 15 x 14 km^2 area. Within this localized volume are located the underpinnings of the active Hengill volcano and fissure swarm, the extinct Grensdalur volcano, and an active high-temperature geothermal field. It was thus expected that the characteristic length scale of heterogeneity would be of the order of a kilometer. In order to image heterogeneous seismic velocity structure at this scale we paid particular attention to the fidelity of the assumed model parameterization, defined as the degree to which the parameterization can reproduce expected structural heterogeneity. We also discuss the trade-off between the resolution of model parameters and image fidelity, compare results obtained from different parameterizations to illustrate this trade-off, and present a synoptic means of assessing image resolution that utilizes the off-diagonal information contained within the resolution matrix. The final tomographic image presented here was determined for a parameterization with fidelity that closely matches the geologic heterogeneity observed on the surface. For this parameterization, the resolution of individual parameters is generally low; however, a quantitative analysis of resolution provides an unambiguous assessment of well-resolved volumes. Within the better resolved regions of the model the averaging volumes are 1-2 km and 2-4 km in vertical and horizontal extent, respectively. Results of tomographic inversion image three distinct bodies of anomalously high velocity, two of these extend from near the surface to a depth of about 3 km. These high-velocity volumes are located directly beneath the surface expressions of the extinct Grensdalur volcano and the extinct Husmuli basalt shield. The third high-velocity structure occurs in the depth range of 3-4 km but does not extend to the surface. These three high-velocity bodies are interpreted to be solidified magmatic intrusions. Relatively low velocities underlay limited portions of the trace of the present accretionary axis and a low-velocity body is imaged in the roots of the active Hengill volcano. The volume of lower velocities located beneath the surface expression of the Hengill volcano is interpreted to be a region of partial melt.

INTRODUCTION

Tomographic inversions of body wave travel time data constrain structural heterogeneity on a broad range of scales. Images of the deep interior of the Earth provide first-order constraints on mantle flow, while crustal images help to constrain local-scale geologic structures. Over this broad range of scales a common question is the resolution of the final model. A less common question is the degree to which a particular model parameterization can faithfully reproduce actual structural heterogeneity, which we consider the fidelity of model parameterization. An example of a model parameterization with inadequate fidelity would be a cellular representation where the cellular dimensions are much greater than those of the actual structural features.

On the scale of 1-100 km, tomographic imaging enables interpretation of remotely sensed crustal and upper mantle heterogeneity in relation to surface geology and tectonics. On these scales the surface expression of geologic phenomena can be particularly variable. The temporal evolution of tectonically and volcanically active areas, for example, may involve spatial migration of the active zone or evolution from a volcanically dominated regime to one marked primarily by nonvolcanic tectonism. Unraveling the history and inferring the dynamics of these environments necessitates images of three-dimensional structure that faithfully map variability of the order of kilometers. Moreover, interpretations of nonunique three-dimensional images of the Earth's inhomogeneities must be guided by quantitative inferences regarding model resolution and fidelity.

In this paper we apply the simultaneous inversion method developed by *Thurber* [1983] to a local earthquake data set collected near the Hengill-Grensdalur central volcano complex, southwest Iceland. We emphasize the importance of model parameterization to image fidelity and resolution. We review the introduction of nonrandom bias by poor model parameterization and the trade-off between resolution of individual model parameters and image fidelity. Examples of inversion results clearly demonstrate the trade-off between fidelity and resolution and that bias may be induced by model representation. The approach to model parameterization and evaluation of image resolution presented here differs from many previously reported studies [e.g., *Aki and Lee*, 1976; *Thurber*, 1983]. We also suggest, based on the empirical comparisons of inversion results, that within the limits of reasonable starting models the tomographic inversions presented here are modestly insensitive to absolute values of velocity. However, the final images and their formal errors provide accurate estimates of relative heterogeneity when properly normalized.

The inversion of the data from the Hengill-Grensdalur area resolves heterogeneous *P* wave velocity structure on the scale of a kilometer in the vertical direction and 2 km in the horizontal

Paper number 89JB01087.
0148-0227/89/89JB-01087$05.00

directions. The tomographic images show well-defined bodies of anomalously high velocity that correlate with structure deduced by other studies [*Foulger*, 1988*a*], in addition to a small low-velocity zone detected beneath the active Hengill central volcano. The high-velocity bodies are interpreted to be solidified magmatic intrusions, and the volume of low velocities is interpreted as a region of partial melt [*Foulger and Toomey*, this issue].

METHOD

Several tomographic techniques exist to analyze body wave arrival time data from local seismometer networks with apertures of the order of 10 km. A recent review of the different methodologies [*Thurber and Aki*, 1987] summarizes the principal distinction between the various methods as the parameterization of the velocity model. This distinction is a critical one in view of the potential for a poor parameterization to yield erroneous results. Heterogeneous earth structure has been parameterized by constant velocity layers [*Crosson*, 1976], constant velocity blocks [*Aki and Lee*, 1976], plane layers constructed of laterally varying blocks with vertically constant velocity [*Benz and Smith*, 1984], analytical functions specified by a small number of parameters [*Spencer and Gubbins*, 1980; *Sharp et al.*, 1980], interpolative functions defined by values specified at nodal points within a three-dimensional grid [*Thurber*, 1983], arbitrarily shaped averaging volumes [*Chou and Booker*, 1979], and continuous functions with a priori probability density distributions [*Tarantola and Nercessian*, 1984]. In some of these cases, it is obvious that model parameterization dictates the geometrical form of the final image. For example, the study of Mount Etna [*Sharp et al.*, 1980] limits the class of models to an ellipsoidal body of anomalous velocity embedded in an otherwise laterally homogeneous crustal structure. For more general model parameterizations, however, a difficulty arises in predicting the mapping function from general three-dimensional structure to the heterogeneity reproduced by a particular parameterization. In this section, we review the relationships between model parameterization, image resolution, and image fidelity that are used in the analysis of the Hengill-Grensdalur data set.

Simultaneous Inversion

The tomographic inversion method utilized in this paper is that developed by *Thurber* [1981, 1983]. Source location parameters and velocity model perturbations are simultaneously estimated from the travel times of P waves from local earthquakes or explosive sources. The technique incorporates three noteworthy components: (1) Parameter separation [*Pavlis and Booker*, 1980; *Spencer and Gubbins*, 1980] is used to decouple hypocenter locations and velocity model perturbations into theoretically equivalent subsets of equations that are computationally manageable. (2) An approximate ray tracing algorithm that requires little computational time is used to estimate minimum travel time paths between specified endpoints [*Thurber and Ellsworth*, 1980; *Thurber*, 1981, 1983]. The utilization of an efficient ray-tracing algorithm permits an iterative solution to the simultaneous inversion problem. Iteration ceases when the ratio of successive travel time residual variances falls below a critical value, as defined by an F test for the 5% level of significance. (3) A velocity model parameterization is used that is capable of rendering a realistic and continuous velocity structure. Of these three components (parameter separation, approximate ray tracing, and velocity model parameterization) only the last requires extensive testing and evaluation for individual data sets in order to achieve good results.

In the case of the Hengill data set we prefer the interpolative method of *Thurber* [1983] for two reasons: (1) The velocity model representation is general and does not assume a specific geometry of structural heterogeneity. (2) The algorithm is suited to the scale of our problem, being capable of imaging anomalous bodies with characteristic dimensions of the order of a kilometer or more.

The method of model parameterization assumes a continuous velocity field by linearly interpolating between velocity values defined at the nodes of a three-dimensional grid. Nodal locations are fixed prior to an inversion, and the spatial distribution of nodes throughout the volume may be irregular. Inversions for heterogeneous structure systematically perturb the values of velocity at the nodal locations. A velocity perturbation depends, in part, on the partial derivative of travel time with respect to a model parameter; the velocity medium partial derivatives are derived directly from the interpolation method. In practice, a critical aspect of this parameterization is the placement and spatial density of nodes within the volume to be imaged.

Effects of Model Parameterization on Image Fidelity and Parameter Resolution

The problem of choosing an acceptable nodal distribution is not unique to Thurber's parameterization. Any imaging problem formulated as parameter estimation, where parameters are nodes, rectangular cells, plane layers, or parameterized functions, must come to terms with the potential for poor image fidelity. Moreover, poor image fidelity is not a benign problem that simply implies, say, a low wave number filter of true heterogeneity. Under-parameterization of a continuously varying, heterogeneous velocity field can give rise to spatial aliasing of structure into the finite dimensional parameter space. *Jackson* [1979] examines parameterized inversions for the functional kernals of integral equations and argues that an important source of nonrandom error, or bias, is the potential for poor fidelity of finite parameterizations. As expected, the effects of bias in a nonlinear inverse problem such as simultaneous inversion are extremely difficult to predict. A comparison of inversion results obtained for different model parameterizations is presented in a later section that illustrates the adverse effects of a poorly parameterized model.

The fidelity of a parameterization trades off with parameter resolution. For a parameterized system the linearized set of equations to solve is

$$\mathbf{y} = \mathbf{A}\,\mathbf{x} + \mathbf{e} \qquad (1)$$

where $\mathbf{y}$ is an n-dimensional vector of travel time delays, $\mathbf{x}$ is an m-dimensional vector of model parameters, $\mathbf{A}$ is the partial derivative matrix that maps model perturbations into travel time delays, and $\mathbf{e}$ is the n-dimensional vector of errors. The error vector is the sum of random errors, such as travel time uncertainties, and nonrandom errors, such as those caused by inadequate parameterization [*Jackson*, 1979]. The Levenburg-Marquardt damped least squares solution $\mathbf{H}$ to equation (1) is

$$\begin{aligned}\mathbf{x}^* &= \mathbf{H}\mathbf{y} = (\mathbf{A}^T\mathbf{A} + \lambda^2\mathbf{I})^{-1}\mathbf{A}^T\mathbf{y} \\ &= \mathbf{V}_p\{(\Lambda_p^2 + \lambda^2\mathbf{I})^{-1}\Lambda_p\}\mathbf{U}_p^T\mathbf{y} \qquad (2)\end{aligned}$$

where A has been replaced by its fundamental decomposition [*Lanczos*, 1961] for the purpose of discussion. $\mathbf{V}_p$ is the $m \times p$ matrix whose columns are the coupled parameter space eigenvectors, $\mathbf{U}_p$ is the $n \times p$ matrix whose columns are the coupled data space eigenvectors, Λ_p is the $p \times p$ matrix of nonzero eigenvalues, $\mathbf{I}$ is the identity matrix, and λ is the damping parameter. The resolution matrix for the damped least squares solution of equation (1) is

$$\mathbf{R} = \mathbf{HA} = \mathbf{V}_p\{(\Lambda_p^2 + \lambda^2\mathbf{I})^{-1}\,\Lambda_p^2\}\mathbf{V}_p^T \tag{3}$$

and the trace of the resolution matrix estimates the degrees of freedom (DOF) intrinsic to the data [*Wiggins*, 1972]:

$$\mathrm{DOF} = \mathrm{tr}(\mathbf{R}) = \sum_{i=1}^{p} \frac{\Lambda_i^2}{\Lambda_i^2 + \lambda^2} \tag{4}$$

Two important properties of a damped least squares inversion are expressed by equation (4). First, in the absence of damping the maximum number of independently resolvable pieces of information equals p, the number of nonzero eigenvalues [*Wiggins*, 1972]. Second, since the degrees of freedom for a given λ is a fixed value less than or equal to p, an increase in the number of model parameters is generally accompanied by a decrease in magnitude of the diagonal elements of $\mathbf{R}$. This would apply only unless it were possible to parameterize the velocity field by p parameters. Thus an increase in the number or density of parameters can simultaneously improve image fidelity and decrease resolution of individual model parameters, as measured by the diagonal of $\mathbf{R}$. This point is clearly demonstrated in a later section by comparing results of simultaneous inversion obtained for two different densities of model parameterization.

In practice, the number of parameters required to faithfully reproduce spatial variations of a seismic velocity field will greatly exceed the number of linearly independent observations, giving rise to nonuniqueness of the final model. This is a well-known problem in geophysical inverse theory [*Backus and Gilbert*, 1970; *Wiggins*, 1972; *Jackson*, 1972, 1979]. The standard approach to solving a nonunique problem is to define averages of model parameters that are well-constrained by a combination of data and a priori assumptions. The weights utilized in this averaging process are defined by the resolution matrix $\mathbf{R}$. The resolution matrix linearly relates actual values of model parameters, in the absence of error, to the estimated values. Each row of the resolution matrix is an averaging vector for a single model parameter [e.g., *Wiggins*, 1972; *Jackson*, 1972, 1979; *Menke*, 1984], and, as such, the row describes the dependence of an estimated parameter value on the values of all other model parameters. Utilizing a large number of parameters in a simultaneous inversion, so as to avoid poor image fidelity and the introduction of biased error to the inverse problem, necessitates examination of the complete averaging vector of each model parameter.

The averaging vector of a model parameter can be pictorially or quantitatively examined. The model parameters in a tomographic inversion have an obvious spatial ordering within the volume to be imaged. An instructive way of examining the resolution matrix is to plot the elements of the averaging vector for a single model parameter in the three-space of the study volume [e.g., *Menke*, 1984]. A qualitative definition of good resolution for a model parameter would be that the weights of the averaging vector were nonzero only in the vicinity of the parameter of interest. Such an averaging vector would be considered compact [*Wiggins*, 1972]. Such plots are presented later in this paper, and they indicate clearly that estimated values of selected model parameters are weighted averages over localized volumes. For a simultaneous inversion with hundreds of nodes, it is impractical to examine pictorially the averaging vector of each node. The definition of a spread function [*Backus and Gilbert*, 1967, 1968; *Menke*, 1984] provides a synoptic view of resolution. For the present problem, we define the spread function for a single averaging vector, following *Menke* [1984], as

$$S(\mathbf{r}_p) = \|\,\mathbf{r}_p\|^{-1} \sum_{q=1}^{m} \Omega(p,q) R_{pq}^2 \tag{5}$$

where $\mathbf{r}_p$ is the averaging vector of the pth parameter, R_{pq} is an element of the resolution matrix, $\Omega(p,q)$ is a weighting function defined as the distance between the pth and qth nodes, and m is the number of parameters. For a compact averaging vector, the spread function is small. By resorting to the spread function to evaluate resolution, some information is lost regarding the directional components of volume averaging. To assess fully the directional nature of averaging, it is still necessary to visually inspect individual averaging vectors. In a later section, we utilize both pictorial representations of selected averaging vectors and the spread function of all averaging vectors to assess the resolving power of the Hengill-Grensdalur data set.

A practical upper limit on the total number of model parameters, however, may be imposed by the distribution of seismic ray paths. In the case of a damped least squares inversion, poorly sampled parameters are generally unperturbed. An overly dense distribution of nodal locations may give rise to localized volumes that are poorly sampled, thus resulting in unresolved and possibly misleading patches of unperturbed velocity. This can be avoided by choosing a nodal configuration with a minimum of poorly sampled nodes.

C. H. Thurber (personal communication, 1986) defines a useful measure of the sampling of nodal locations, the derivative weight sum (DWS). The DWS provides an average relative measure of the density of seismic rays near a given velocity node. This measure of seismic ray distribution is superior to an unweighted count of the total number of rays influenced by a model parameter, since it is sensitive to the spatial separation of a ray from the nodal location. The DWS of the nth velocity parameter α_n is defined as

$$\mathrm{DWS}(\alpha_n) = N \sum_i \sum_j \left\{ \int_{P_{ij}} \omega_n(\mathbf{x})\, ds \right\} \tag{6}$$

where i and j are the event and station indices, ω is the weight used in the linear interpolation and depends on coordinate position, P_{ij} is the ray path between i and j, and N is a normalization factor that takes into account the volume influenced by α_n. The magnitude of the DWS depends on the step size of the incremental arc length ds utilized in the numerical evaluation of equation (6). Smaller step lengths yield larger DWS values; therefore, DWS provides only a relative measure of ray distribution and its units of distance are unimportant. Poorly sampled nodes are marked by relatively small values for the DWS. In practice, it is useful to monitor changes in the spatial variation of the DWS while testing for an optimum nodal configuration. A good parameterization, in general, maximizes the number of parametric nodes within a volume and, for a damped least squares inversion, minimizes the number of poorly sampled nodes.

It is worth noting that a nonlinear stochastic inversion [*Tarantola and Valette*, 1982] or smoothing constraints [*Parker*, 1975; *Sabatier*, 1977] would relax the upper limit on the density of nodes imposed by a damped least squares inversion. For the Hengill-Grensdalur data set, however, the seismic ray distribution is sufficiently good to allow a close spacing of nodal locations that is acceptable for reproducing expected velocity heterogeneity while simultaneously minimizing the number of poorly sampled nodes.

The approach to model parameterization discussed in this section contrasts with many previous studies. We are advocating that resolution of individual model parameters is less important than employing a model parameterization that possesses good fidelity. Since parameterizations with good fidelity may often result in significant nonuniqueness in the estimates of individual model parameters, we have adopted a methodology that permits quantitative evaluation of the degree of nonuniqueness, or volume averaging of velocity. The relationships reviewed in this section are not particularly new ones; however, in the case of the Hengill-Grensdalur study we demonstrate below that model fidelity has profound influence on the final results of inversion and that the relationships discussed here are vital to the evaluation of the spatial extent of well-resolved volumes.

THE HENGILL-GRENSDALUR CENTRAL VOLCANO COMPLEX, ICELAND

The Hengill-Grensdalur central volcano complex forms part of a ridge-ridge-transform triple point in southwestern Iceland (Figure 1). It contains the presently active Hengill central volcano, of Pleistocene to Recent age, and the extinct Grensdalur central volcano [*Foulger*, 1988*a*], in addition to other more minor eruptive sites. The volcanic history, discussed in more detail by *Foulger and Toomey* [this issue], has involved the migration of volcanism and the accretionary axis over approximately the last 1 m.y. Lateral structural inhomogeneity is likely in such an evolving tectonic setting, and it was expected that detailed definition of the crustal structure heterogeneity would aid in interpreting the volcanic history of the area.

A high-temperature geothermal area encompasses the central volcano complex and is characterized by continuous, small-magnitude earthquakes [*Foulger*, 1988*a*]. Many of these events are induced by the process of cooling contraction within the heat source of the geothermal area [*Foulger*, 1988*b*]. This activity was investigated in a 4-month experiment during the summer of 1981. During this period a 23-station network of short-period vertical seismometers was in operation (Figure 2). The nominal separation between adjacent stations was 3-5 km, and the network aperture

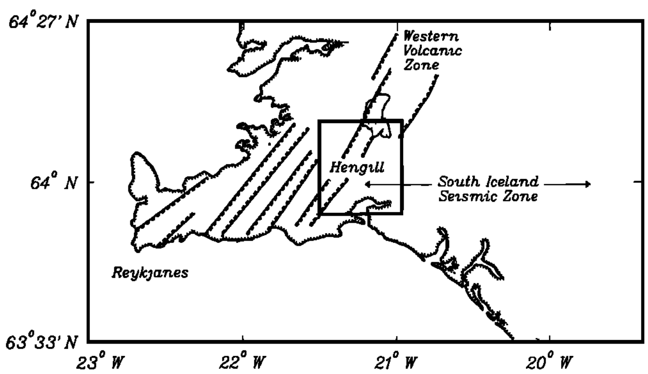

Fig. 1. Map of principal tectonic features in southwestern Iceland, after *Einarsson and Bjornsson* [1979]. The position of the South Iceland Seismic Zone is shown schematically; zones of fissure swarms are outlined by parallel saw-toothed lines; lakes are stippled. The bold rectangle defines the area of the 1981 Hengill-Grensdalur microearthquake survey that is shown in Figure 2.

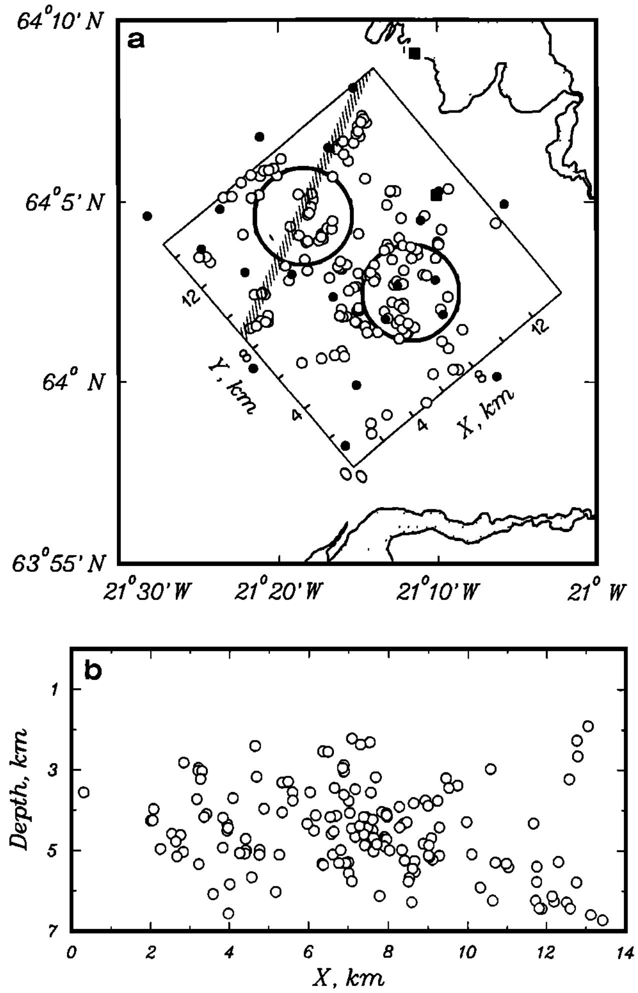

Fig. 2. (*a*) Surface location of volcanic centers and accretionary axis with epicenters, seismic stations, and shot locations used in the tomographic analysis. The two larger circles and the hachured line schematically show positions of the Hengill and Grensdalur volcanoes and the present axis of accretion, respectively. The recently active Hengill volcano and the extinct Grensdalur volcano are to the northwest and southeast, respectively. Smaller solid circles represent seismic stations; open circles denote microearthquake epicenters; solid squares show the two shot locations. The origin of the coordinate system used in simultaneous inversion is the southernmost corner of the rectangle; the origin of the z axis is at sea level. Shaded areas are lakes and rivers. (*b*) Projection of microearthquake hypocenters used in the tomographic inversion onto a vertical plane parallel to the x axis of Figure 2*a*.

was 15 km. Since the spatial and temporal distribution of the activity was known to be relatively constant from a previous investigation [*Foulger and Einarsson*, 1980], a network configuration was used that would provide good azimuthal coverage of the abundant, small-magnitude seismicity.

ARRIVAL TIME DATA

The highest-quality P wave arrival times were selected from a data set that includes 1918 earthquakes and five explosive sources [*Foulger*, 1988*a*]. Earthquake hypocenters were located using the arrival times of impulsive P waves, which could be read to an estimated precision of 0.01 s. Because of instrument and clock corrections, however, the overall uncertainty of the travel times is conservatively estimated to be ±0.03 s at the one standard deviation level of confidence. Earthquake locations were determined by *Foulger* [1988*a*] under the assumption of a laterally homogeneous velocity structure, constrained by refraction data [*Palmason*, 1971; *Angenheister et al.*, 1980], using the computer algorithm HYPOINVERSE [*Klein*, 1978].

The large quantity and variable quality of the arrival time data permitted the selection of a high-quality data subset for the inversion. This was done by winnowing out poorly located events, under the assumption that these resulted from relatively poor quality or a limited number of arrival time estimates. Criteria applied for this winnowing were as follows: (1) Epicentral and station locations were restricted to the 14 x 15 km^2 area central to the seismic network and shown by the rectangle in Figure 2. The crustal volume to be imaged underlies this area. (2) Events selected were located using at least 12 reliable arrival times. (3) Uncertainties in epicentral position and focal depth were less than 1.0 and 2.0 km, respectively. (4) The total rms travel time misfit for each event was less than 0.10 s. (5) The maximum gap in source-to-receiver azimuth [*Klein*, 1978] was less than 180°. (6) The epicentral distance of the station nearest the event was less than twice the focal depth. We selected 303 events using these criteria.

The hypocenters of the 303 well-located and -recorded events were not uniformly distributed throughout the volume to be imaged. To improve the uniformity of sampling, the data set was narrowed further to remove redundant events within regions of dense activity. Four earthquakes were also added in areas of sparse seismicity. These four additional events fulfilled the constraints listed above except the minimum number of arrival times was lowered to nine. This sorting process reduced the total number of earthquake sources to 158. The epicentral and hypocentral distribution of these sources are shown in Figures 2*a* and 2*b*. Travel times of two shots (Figure 2*a*) were also included in the inversion data set.

Twenty of the 23 available stations were used for arrival times (Figure 2*a*), the three remaining stations being located well outside the study area. In all, a total of 2409 *P* wave arrival times constituted the data set used for the tomographic inversion. The hypocentral parameters of the final set of 158 earthquakes, obtained with the laterally homogeneous velocity model, served as the initial source locations prior to inversion. The two shot positions and origin times were held fixed throughout the inversion.

APPLICATION OF SILMUTANEOUS INVERSION

Initial Values and Nodal Placement

The final three-dimensional velocity structure determined by the simultaneous inversion method of *Thurber* [1983] depends on ray coverage, data uncertainty, a priori values for hypocentral parameters, and velocity model parameterization, including the placement and density of nodal points and initial velocity structure. For the Hengill-Grensdalur study, travel time data quality is good; one standard deviation arrival time errors are approximately 0.03 s, and the distribution of sources and stations provides extensive ray coverage (Figure 2).

Initial estimates of hypocentral and velocity model parameters should be reasonably close to the final values, in order to reduce the effects of nonlinearity. A natural choice of hypocentral parameters was those originally calculated using HYPOINVERSE and the assumed laterally homogeneous velocity model [*Foulger*, 1988*a*]. The combination of excellent station distribution in the Hengill area and the relatively small degree of expected velocity

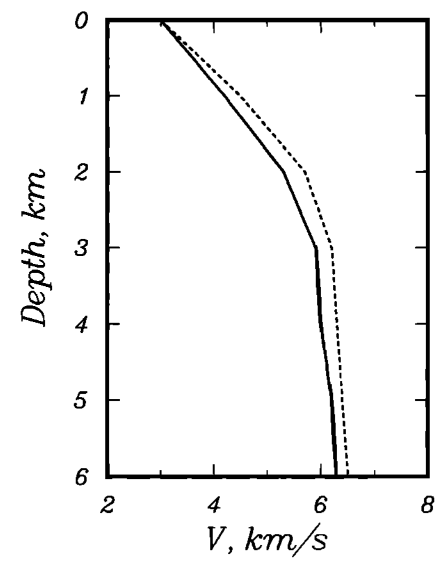

Fig. 3. *P* wave velocity depth models used to initialize simultaneous inversions. The solid curve indicates the regional model used by *Foulger* [1988*a*] to locate the events. The dashed curve is a lateral average of several test tomographic inversions.

heterogeneity (see below) suggested that these were good starting values for the simultaneous inversion. Prior to perturbing the initial velocity structure, these initial hypocentral parameters are recalculated so as to avoid any possible bias between HYPOINVERSE and the simultaneous inversion routine.

Regional refraction profiles in southwest Iceland [*Palmason*, 1971] provided good constraint on the laterally averaged *P* wave velocity structure. Steep velocity gradients (1 s^{-1}) are present at shallow depths (0-3 km), lower-velocity gradients (0.1-0.2 s^{-1}) from 3 to 10 km depth. A half-space velocity of 7.0 km/s is derived from the results [*Angenheister et al.*, 1980]. These data were modelled by *Foulger* [1984] using the program TTGEN [*Klein*, 1978] to obtain the velocity depth function shown in Figure 3 (solid line). Also shown in Figure 3 (dashed line) is a second velocity-depth function which is a lateral average of several trial tomographic inversions conducted to explore nodal configuration. The higher velocities are consistent with the observations of *Palmason* [1971] and *Flovenz* [1980] that suggest higher than average velocities near Icelandic central volcanos. Both velocity depth structures were tested as starting models for the simultaneous inversion.

The choice of a starting model for inversion for three-dimensional structure depends upon the degree of crustal velocity heterogeneity. In extremely heterogeneous areas it is often beneficial to step progressively from one- to two- to three-dimensional models [*Thurber*, 1983]. Such an approach minimizes the chance of poor convergence caused by a starting model that is not sufficiently close to the structure of the actual Earth. *Foulger* [1984] and *Foulger and Toomey* [this issue] examined travel time delays from teleseismic events and regional explosions and found that the anomalies were consistent with lateral velocity variations of 5-10%. The magnitude of the expected heterogeneity of velocity within the Hengill-Grensdalur area therefore suggested that determination of an intermediate two-dimensional model was unnecessary. The rapid convergence and consistency of all attempted simultaneous inversions verified this.

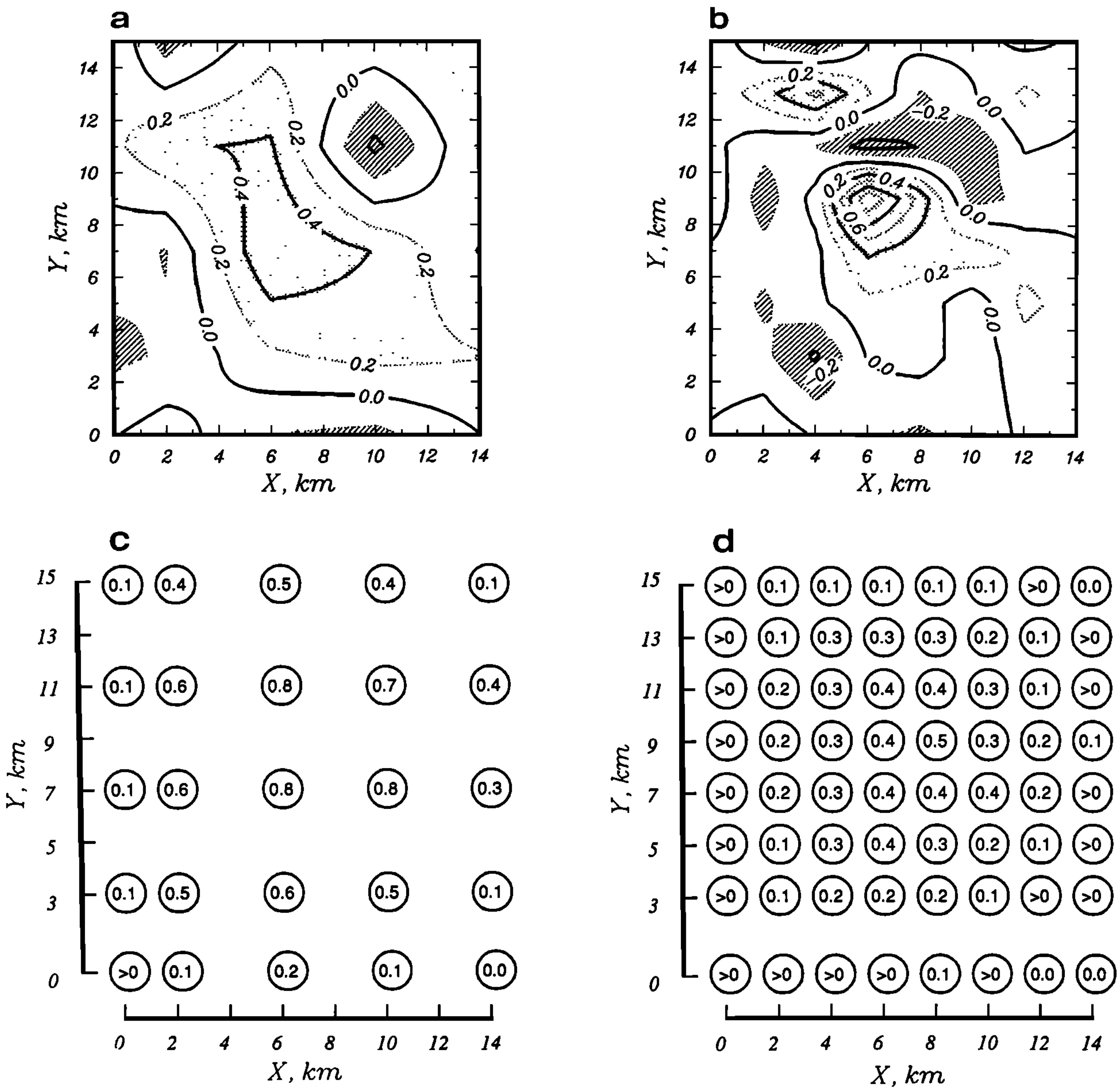

Fig. 4. A comparison of results obtained for coarse and fine parameterizations along with the distribution of model parameters and values of resolution (see text for discussion of parameterizations). (*a*) (*b*) The contour plots of normalized velocity perturbations are for the horizon of nodes at 3 km depth; the contour interval is 0.2 km/s. Stippled and hachured areas are >0.2 and <-0.2 km/s, respectively. (*c*) (*d*) The resolution of an individual model parameter, as measured by the diagonal of the resolution matrix, is plotted at the location of a parametric node. Nonzero values of resolution that are less than 0.05 are indicated as >0.

Several nodal configurations were tested for the velocity parameterization to determine the preferred configuration. In a series of test inversions, the horizontal and vertical separation of nodes was varied from 2 to 4 km and 1 to 2 km, respectively. The results of simultaneous inversion for all nodal configurations were in general agreement in that the structural image remained broadly stable. However, coarse nodal spacing (4 and 2 km in the horizontal and vertical directions, respectively) led to solutions displaying much broader regions of anomalous velocity, whereas finer nodal spacing (2 and 1 km in the horizontal and vertical directions, respectively) resulted in the definition of distinct bodies of anomalous velocity. More importantly, the precise location of some bodies of anomalous velocity were noticeably different between the two parameterizations, as discussed below. The final rms travel time residual for the finer nodal spacing was significantly smaller than that of the coarser nodal spacing (by 0.01 s), a difference significant at 95% confidence as determined by an *F* test. This statistically significant reduction of rms travel time residuals strongly suggests that the finer nodal spacing yielded the better results.

A closer examination of the differences between the final models obtained from the coarse and fine parameterizations demonstrates the importance of nodal placement and the trade-off between image fidelity and model resolution. Figures 4*a* and 4*b* show the results of simultaneous inversion for nodes at 3 km depth for the coarse and fine parameterizations, respectively. Beneath each contour plot of velocity is shown the distribution of model parameters at 3 km depth and the resolution as measured by the diagonal of the resolution matrix (Figures 4*c* and 4*d*). Both results were obtained from identical data and starting models, the only difference being

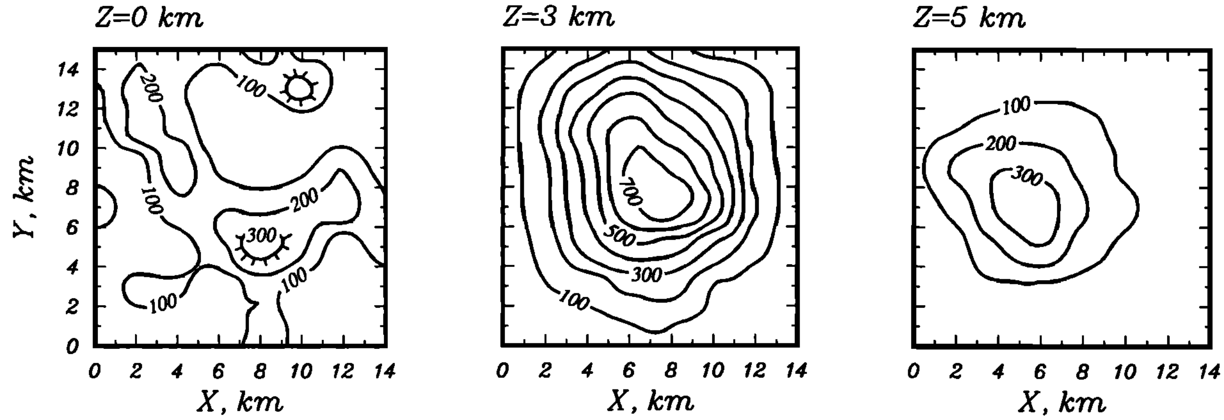

Fig. 5. Plan view contour maps of the derivative weight sum (DWS) at selected depths of 0, 3, and 5 km. See Figure 2 for the orientation of x and y axes. The contour interval is 100.

the density of model parameterization. The first-order differences between the two results were the location of a body of anomalously low velocity and the resolution of individual parameters. For the coarse parameterization (Figures 4*a* and 4*c*), a well-resolved node located at x=10, y=11 km defined the low-velocity body. The resolution of this parameter as measured by the diagonal element of the resolution matrix was 0.7. For the finer nodal spacing (Figures 4*b* and 4*d*), the lowest velocity observed at 3 km depth was located at x=6, y =11 km. The resolution of this model parameter as measured by the diagonal element of the resolution matrix was 0.4. Also note the overall change in the shape of the low-velocity region. In both cases, the model parameters comprising the horizon at 3 km depth, including the region of observed low velocities, were amongst the best resolved parameters in their respective inversions, again according to the diagonal element of the resolution matrix. In agreement with the discussion presented in an earlier section, we observed that an increase in the density of model parameters, which unequivocally translates to improved model fidelity, was accompanied by a decrease in the resolution of all individual parameters. This result comes as no surprise. What is noteworthy, however, is the observation that the two models differ by 4 km in their estimate of the location of the low-velocity body. These results suggest that in the case of this study, a change in the fidelity of parameterization gives rise to significantly different results. The important question to be resolved is which of these two models, if either, is acceptable.

We argue that the finer model parameterization, which has improved model fidelity but decreased resolution of individual model parameters, yields superior results compared to the sparse parameterization. Following *Wiggins* [1972], we rest our argument on the following facts: the addition of model parameters gave rise to a statistically significant decrease in the a posteriori variance of travel time residuals, and the trace of the resolution matrix for the finer parameterization was significantly larger than for the sparse nodal distribution. The trace of the resolution matrix for the coarse and fine parameterizations was approximately 26 and 46, respectively. Thus, since the data contain independent information relevant to the additional parameters included in the finer parameterization, these parameters must be important to the problem . We further argue that the degradation of resolution of individual model parameters, as measured simply by the diagonal of the resolution matrix, is a misleading statistic since it ignores off-diagonal information. With regards to resolution, the important matter to be considered is the volume over which velocity is averaged when estimating the value of a model parameter. In the case of the sparse parameterization, the resolving kernal for the node that defined the low-velocity body indicated that volume averaging was principally restricted to the region influenced by the node under question. However, given that coarse nodal spacing was 4 and 2 km in the horizontal and vertical directions, respectively, it is clear that the averaging volume is large. For the finer parameterization, the resolving kernals, as discussed at length below, indicated that the estimated value of a model parameter depends on neighboring nodes to some degree. However, for the finer parameterization the nodal separation was only 2 and 1 km in the horizontal and vertical directions, respectively, so it appears that volume averaging is limited to a smaller, or at least comparable, volume compared to the sparse parameterization. Thus we see that even though the finer model parameterization results in smaller diagonal elements in the resolution matrix, it may actually imply a lesser amount of volume averaging of velocity. We attribute the differences between the inversion results (Figures 4*a* and 4*b*) to spatial aliasing caused by the introduction of biased error in the case of the sparse parameterization. It follows from these comparisons that, in the case of the Hengill-Grensdalur study, a large value along the diagonal of the resolution matrix is a potentially poor discriminant of the significance of imaged anomalies.

To determine if the finer parameterization of 2 and 1 km in the horizontal and vertical directions, respectively, possessed adequate fidelity, we conducted a single iteration for a model with nodal parameters spaced at 1 km in all coordinate directions from 0 to 5 km depth. This model included 1050 parameters, and the nodal spacing of 1 km was roughly twice the seismic wavelength. This single iteration permitted us to approximately evaluate the trace of the resolution matrix, and its value was 56. This suggests that the Hengill-Grensdalur data do contain structural constraints that are not fully exploited by a parameterization that is greater than 1 km in all coordinate directions. This very dense parameterization, however, was not explored further for the reason that the sampling distribution of ray paths measured by DWS was irregular, causing many nodes in the interior of the model to be inadequately constrained by seismic rays. Recall that for a parameterization with nodes spaced at 2 and 1 km in the horizontal and vertical directions, respectively, the trace of the resolution matrix was 46, suggesting that over 80% of the available information was utilized. We do not

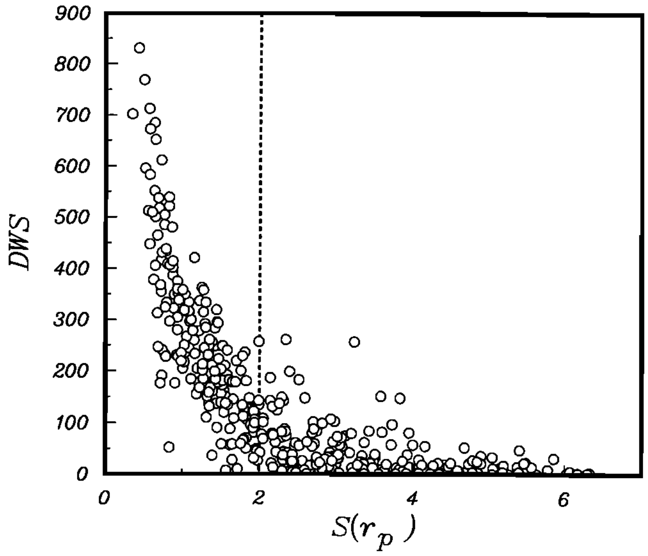

Fig. 6. A plot of the DWS versus the spread function of the averaging vector for each of the 448 model parameters. The dashed line at $S(\mathbf{r}_p)$=2 is the upper limit for values of the spread function considered to be acceptable (see text for explanation).

completely dismiss, however, the potential for spatial aliasing on a scale of 1-2 km in the final model, and the interpretation of the tomographic image takes this into consideration.

The nodal distribution used for the final inversion involved nodes spaced at 2-km intervals in the horizontal direction, except for a 3-km spacing between rows near the southern edge at y=0 and y=3 km. Nodal spacing in the vertical direction was 1 km from 0 km (sea level) to 6 km depth. A total of 448 nodes therefore sampled the 14 x 15 x 6 km^3 volume. Plan view contour plots of the DWS are shown in Figure 5 at depths of 0, 3, and 5 km. These plots illustrate that nodes at the intermediate depth of 3 km are evenly and well sampled by ray paths. The distribution of the DWS at 0 km depth shows marked lateral variability when compared with the plot for 3 km depth, a natural result of recording on a discrete array of stations (Figure 2a). Large values (good sampling) therefore occur directly beneath stations, and small values (poor sampling) occur in regions of sparse network coverage. At a nodal depth of 5 km the DWS decreases as a result of the fall off of seismicity with depth (Figure 2*b*). Overall, inspection of the DWS contour plots for all nodal depths between 0 and 6 km indicated that away from the edges of the 14 x 15 km^2 area and from the depths of 1-5 km the distribution of seismic ray paths was adequate to resolve structural variations on the spatial scale defined by the nodal distances.

Resolution of Model Parameters

Given a nodal configuration and an estimate of ray path distribution, we can evaluate the resolution matrix and the spread function of each averaging vector. For the following analysis of resolution, we used our inversion results, presented below, to calculate the seismic ray paths.

The spread function $S(\mathbf{r}_p)$ (equation (5)) was evaluated for the averaging vector of each model parameter. Figure 6 shows a plot of the DWS versus the spread of the averaging vector for each of the 448 model parameters. As expected, well-sampled nodes (large DWS) generally correspond to smaller values of $S(\mathbf{r}_p)$. Since an averaging vector depends on the geometry of rays near a node, and not just the total number or density of rays *Aki et al.* [1977], there is significant scatter about the general trend apparent in Figure 6. The scatter suggests that resolution studies based on just the total number of times a parameter is sampled by rays are qualitatively correct.

A subjective choice of the range of acceptable values of the spread function is assisted by examining the individual averaging vectors. An acceptable averaging vector, or spread function value, should indicate localized averaging of velocity. Figures 7 and 8 show three-dimensional perspective plots of two averaging vectors in the study volume; the values of the elements of each averaging vector are plotted at the nodal location corresponding to that element.

The averaging vector in Figure 7 is for a node in the center of the volume (x=8, y=7, and z=3 km). The spread of the averaging vector for this node is 0.3. This averaging vector is clearly compact, indicating localized averaging of velocity. Figure 8 displays the averaging vector for a node at x=2, y=3, and z=2 km. The spread of the averaging vector for this node is 1.9. Inspection of the averaging vector of Figure 8 indicates significant amounts of vertical averaging of velocity between 0 to 3 km depth and, to a lesser degree, horizontal averaging of velocities within ±2 km of the node in question. We consider the averaging vector of Figure 8 and its value of spread to be just acceptable for the following reasons: (1) it is compact, indicating volume averaging that is centered about the desired node, and (2) we interpret the final velocity anomalies on a scale of several kilometers; that is, we do not attribute geologic importance to the velocity anomaly at any single parameter. Thus our interpretation is biased toward

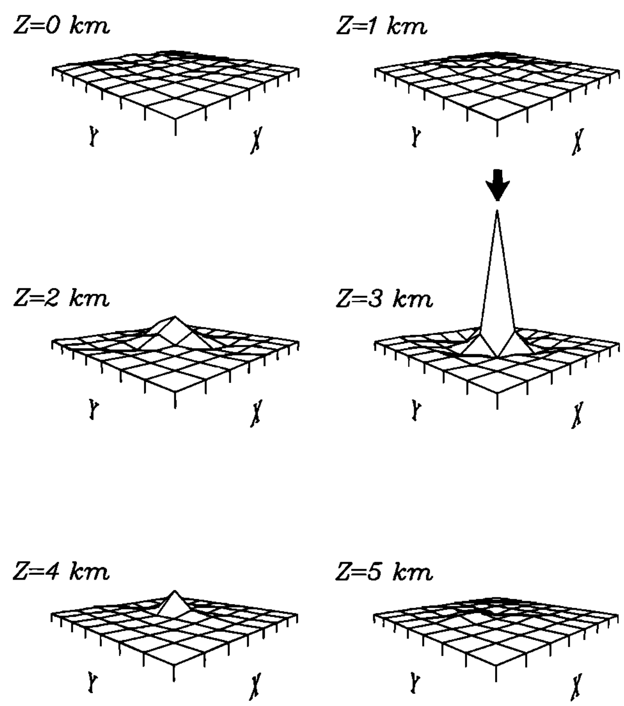

Fig. 7. Three-dimensional perspective plots of the averaging vector for the node located at x=8, y=7, and z=3 km, which is indicated by arrow. The orientation of the x and y axes are shown in Figure 2. The values of the elements of the averaging vector are plotted at the nodal location corresponding to that element. Six perspective plots are shown, one for each horizon of nodes between 0 and 5 km depth. Within a perspective plot for a single depth the corners of a quadrangle correspond to one of the 64 nodal locations within a horizontal plane.

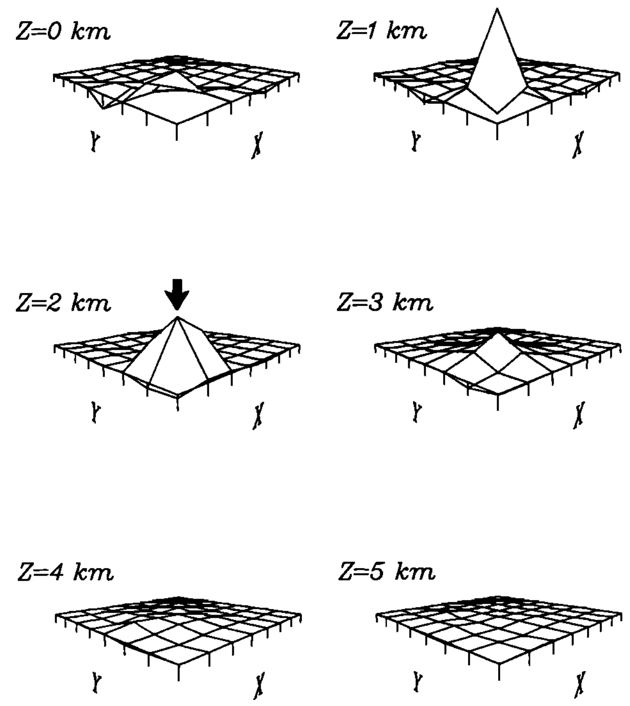

Fig. 8. A three-dimensional perspective plot of the averaging vector for the node located at x=2, y=3, and z=2 km. See Figure 7 for further explanation. The vertical scales of Figures 7 and 8 are identical.

anomalies which are clearly defined on a scale that is spatially larger than the averaging volumes associated with the parameters that define the anomalies. On the basis of pictorial examination of numerous averaging vectors, we chose for this study a spread value of 2 as an upper limit for the range of acceptable values of $S(\mathbf{r}_p)$. Naturally, the smaller the value of $S(\mathbf{r}_p)$, the smaller the volume is through which velocity is averaged. The upper limit of 2 for $S(\mathbf{r}_p)$ is not a universal value applicable to all studies but simply a value that indicates acceptable resolution in the case of the Hengill-Grensdalur study. Figures 9*a* and 9*b* show plan view contour plots of $S(\mathbf{r}_p)$ at nodal depths between 0 and 5 km depth alongside plots of normalized velocity perturbations. Areas where $S(\mathbf{r}_p)$ is less than 2 are considered to be adequately resolved.

Variance Reduction and Model Error

Simultaneous inversions were conducted for both of the velocity depth functions shown in Figure 3. For an inversion initialized with the velocity model of *Foulger* [1988*a*], hereafter referred to as inversion 1, the initial rms travel time residual was 0.06 s. For inversion 2, which was initialized by the second velocity-depth function of Figure 3, the initial rms travel time residual was 0.05 s. In both cases the initial rms travel time residual was calculated after the first relocation of hypocenters but before velocity model perturbation. Iteration of the complete simultaneous inversion terminated after 4 and 3 steps for inversions 1 and 2, respectively. In both cases, the final rms travel time residual was 0.04 s. The travel time residual variance reduction for inversions 1 and 2 was 46% and 37%, respectively. An F test on the ratio of the final travel time variance from the two inversions indicates that the overall travel time misfits are indistinguishable at the 5% level of significance. With respect to the final variance of travel time residuals, the inversion results are therefore statistically independent of the initial velocity model.

A comparison of the final heterogeneous velocity structures does indicate a minor dependency on the initial model. The following assumptions are made in the discussion of model error: First, the statistics are only approximately correct since the problem is nonlinear. Second, since the resolution and covariance matrices are similar except for a scaling factor and we limit our discussion to well-resolved nodes, the magnitude of covariance between a given model parameter and all others is smaller than the variance of the model parameter. This assumption is generally true for $S(\mathbf{r}_p) < 2$, allowing us to simplify the discussion. Third, the a posteriori variance estimates of well-resolved model parameters [*Thurber*, 1981, 1983] should give approximate limits for acceptable differences between the final models of inversions 1 and 2. For both inversions, the mean standard error of fractional perturbations, defined as the percent deviation from the starting model, was 2%. This average value is equivalent to an error of about 0.1 km/s in the final estimate of velocity at a node. We evaluated the difference between the final models using several different comparisons. Simply subtracting the final velocity values obtained from inversion 2 from those of inversion 1 for all well-resolved nodal locations ($S(\mathbf{r}_p) < 2$) suggested a minor dependency on the initial model; the mean and the rms difference between the final velocity models being -0.1 and 0.2 km/s, respectively. The negative mean indicates that the offset of the two final models has the same sign as the offset of the starting models; that is, velocities from inversion 2 were systematically greater than velocities from inversion 1. A similar dependency of the final velocity model on the initial model has been observed previously [e.g., *Eberhart-Phillips*, 1986]. We then subtracted the respective initial model from each final model and compared these velocity perturbations for all well-resolved nodal locations. The mean and the rms of the difference between these velocity perturbations were both 0.2 km/s. The positive mean indicates that perturbations for inversion 1 were generally greater than those of inversion 2. This result is expected since the initial model of inversion 2 already included some results of previous inversions.

As a final test, for each inversion and for each horizontal layer of nodes, the average velocity was calculated for the final structure. Again, only well-resolved nodes were included in this averaging process. These average velocity-depth structures were then subtracted from their respective final models, yielding normalized velocity perturbations. The mean and the rms difference between the two sets of normalized velocity perturbations was 0.0 and 0.1 km/s, respectively, showing good agreement between the two normalized models.

These comparisons suggest that the final velocity field may be modestly biased by the choice of the starting model. However, velocity perturbations relative to a lateral average of the final model are apparently unbiased by the initial model. This result suggests that for the Hengill-Grensdalur data set the normalized three-dimensional structural variations calculated from simultaneous inversion are, within the limits of acceptable initial models, insensitive to absolute initial values of velocity. The minor dependency of final absolute velocities on the starting model may result from a trade-off between hypocentral parameters and unresolved velocity structure [e.g., *Pavlis and Booker*, 1983].

Results

The results of inversion 2 are presented in Figures 9*a* and 9*b*. In Figures 9*a* and 9*b* we depict plan view contour plots of normalized velocity perturbations at nodal depths between 0 and 5 km.

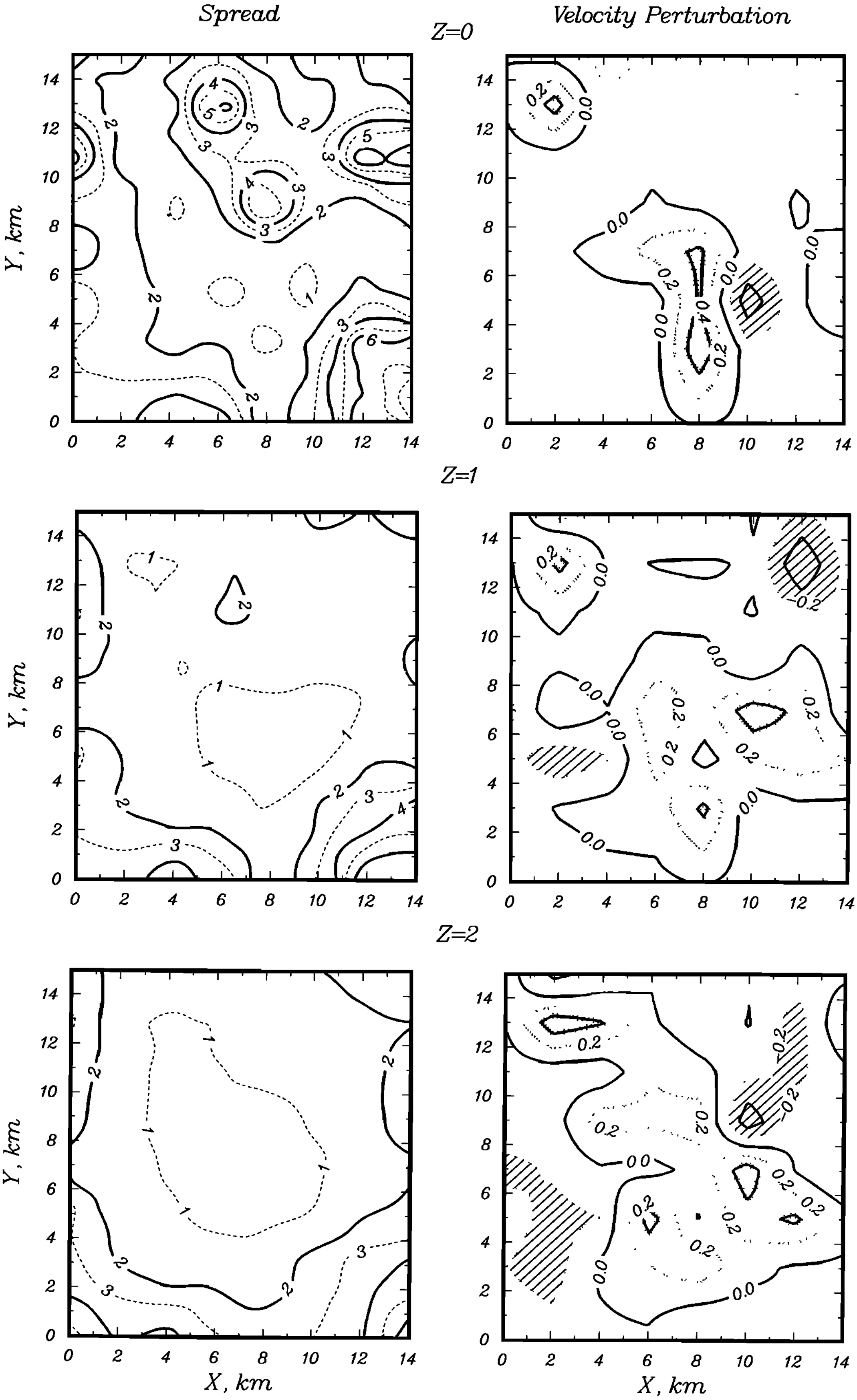

Fig. 9*a*. Plan view contour plots of spread and normalized velocity perturbations at nodal depths of 0, 1, and 2 km. The orientations of the *x* and *y* axes are shown in Figure 2. The contour interval for the plots of $S(\mathbf{r}_p)$ is 1. Regions where $S(\mathbf{r}_p)$ is less than 2 are considered to be well resolved. The contour interval for normalized velocity perturbations is 0.2 km/s, and the stippled and hachured areas are >0.2 and <-0.2 km/s, respectively.

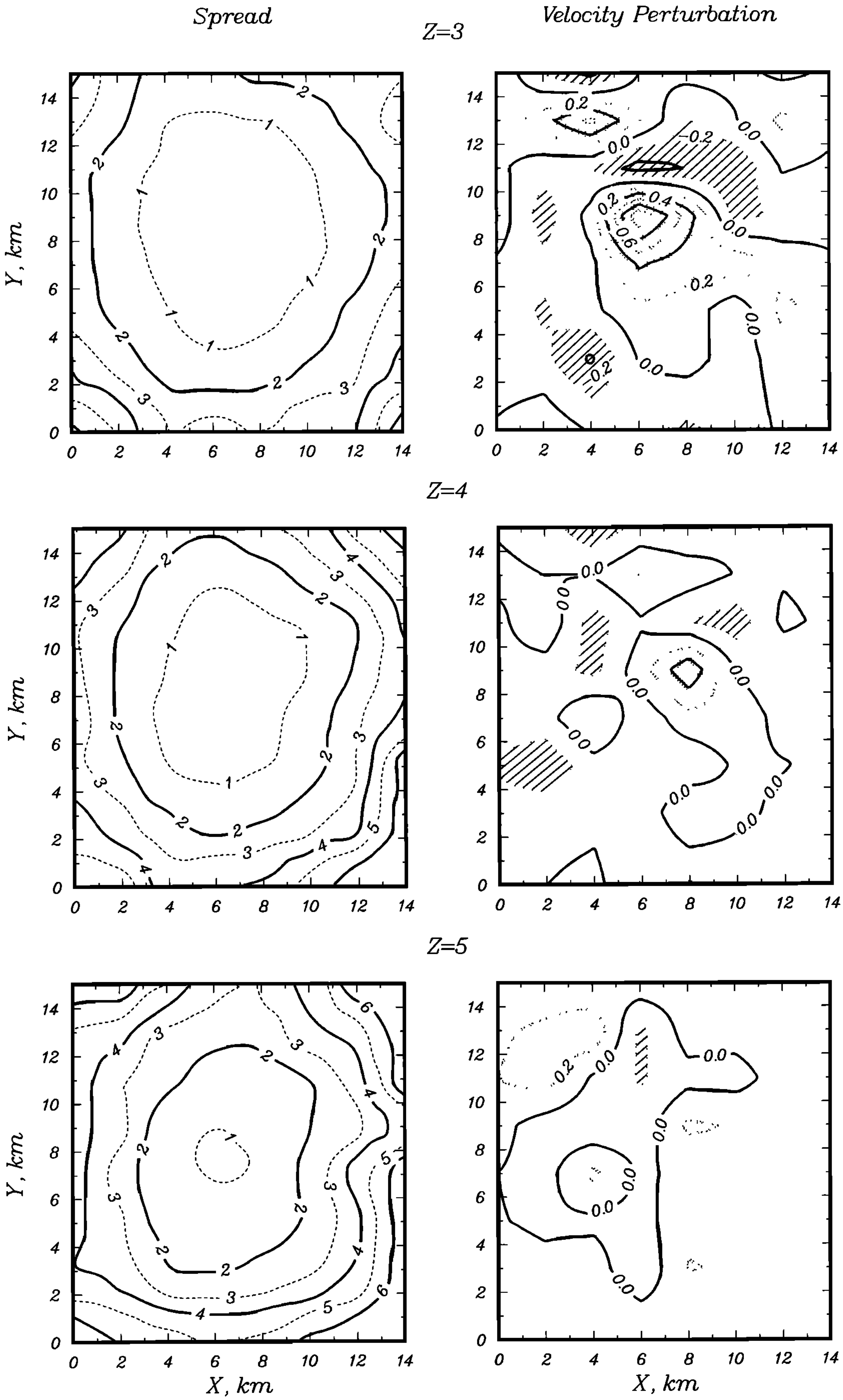

Fig. 9b. Plan view contour plots of spread $S(\mathbf{r}_p)$ and normalized velocity perturbations at nodal depths of 3, 4, and 5 km. Nodes at 6 km depth were poorly resolved; that is, $S(\mathbf{r}_p)$ was everywhere greater than 2

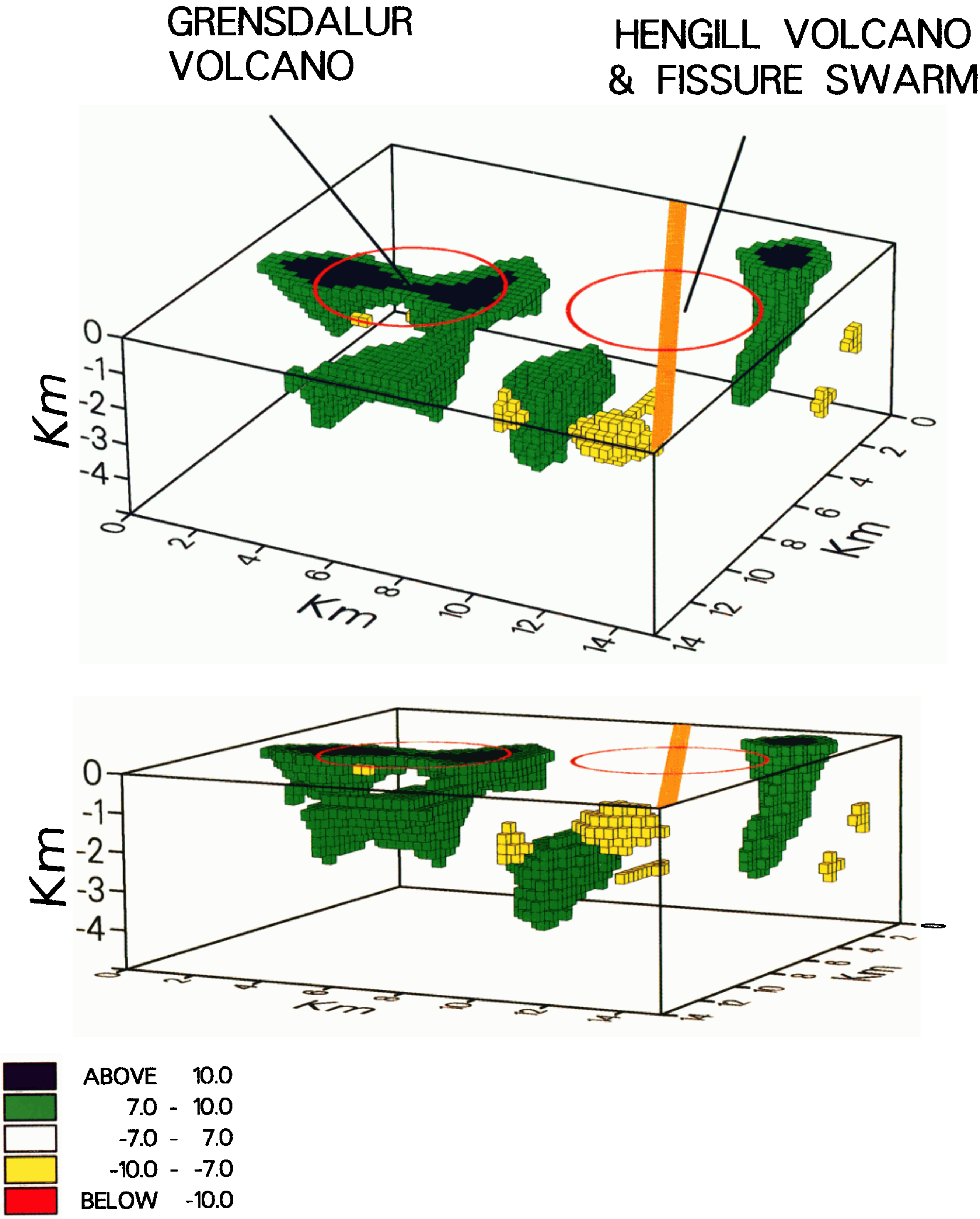

Plate 1. Three-dimensional images of the inversion results. The color scale denotes percentage difference in velocity from the regional structure (Figure 3, solid curve). For display purposes, the model is represented by constant-velocity cubic blocks of dimension 0.25 km; the actual inversion solution, as described in the text, defines velocity by continuously interpolating between parametric nodes. Two separate views of the solution are shown; both views are from the northeast. Positions of the surface expressions of the Grensdalur and Hengill volcanoes (red circles) and the axis of accretion (solid bar) are from *Foulger* [1988*a*]. See Figure 2 for a map view.

Structure below a depth of 5 km was unresolvable. The contour interval for the plots is 0.2 km/s and exceeds the estimate of the standard error of the velocity perturbations. Shown alongside each contour plot of normalized velocity perturbation is the contour plot of the spread $S(\mathbf{r}_p)$ for the associated horizon of nodes. As stated above, only regions where $S(\mathbf{r}_p) < 2$ are considered to be well resolved. The plots summarize the distribution of well resolved velocity anomalies. For example, inspection of Figure 9*a* at a depth of 0 km shows that two near-surface velocity anomalies are clearly within areas in which $S(\mathbf{r}_p) < 2$. However, in some regions the lateral extent of these bodies (at 0 km depth) is poorly resolved since the zero contour of velocity perturbation occurs where $S(\mathbf{r}_p) > 2$. For the 3-km depth contour plot (Figure 9*b*), pronounced lateral variability of crustal structure is detected. The contour plots of $S(\mathbf{r}_p)$ at this depth show that most of these velocity anomalies lie within regions with $S(\mathbf{r}_p) < 1$, indicating good resolution.

The final three-dimensional model is characterized by several distinct bodies of anomalously high velocity. At shallow (0-2 km) crustal depths, Figure 9*a* shows two prominent velocity highs centered at approximately x=2, y=13 km and x=8, y=5 km, respectively. In the core of these anomalies, velocities are greater than the average structure by approximately 10%. Less well defined velocity lows were observed at shallow depths at x=12, y=13 km and x=10, y=9 km, where the maximum deviation from the average model is again about -10%. The most pronounced velocity anomalies are centered at a depth of 3 km (Figure 9*b*). The anomaly at x=8, y=5 km does not extend to this depth, but the anomaly centered near x=3, y=13 km is still present. A third well-defined high-velocity anomaly is observed centered on x=6, y=9 km, at this depth. Within this structure velocities are higher than the average by more than 15%. This anomalous volume extends to a depth of 4 km. The two high-velocity bodies present at 3 km depth are distinct and separated by a narrow zone of relatively low velocities with a maximum deviation from the average structure of approximately -7%.

The spatial separation of distinct velocity anomalies and the vertical coherence of imaged bodies is best illustrated in the perspective views of Plate 1. In these views the velocity perturbations are expressed as percent deviations from the regional velocity depth function derived from the analysis of refraction data (Figure 3, solid curve). Also plotted on the surface planes of Plate 1 are the locations of the extinct Grensdalur volcano, the presently active Hengill volcano, and the axis of the fissure swarm which marks the present locus of crustal spreading. The three distinct bodies of anomalously high velocities are clearly present in this figure. The two high-velocity volumes extending from the surface to approximately 3 km depth are associated with the extinct Grensdalur volcano and a region approximately 3 km west of Hengill. The third high-velocity body, at a depth of 3-5 km, is located midway between the two volcanoes. The maximum depth of this anomaly is not well constrained due to poor resolution deeper than 5 km (Figure 9*b*). All three of these high-velocity bodies are interpreted to be solidified magmatic intrusions into the upper crust [*Foulger and Toomey*, this issue]. The low-velocity bodies imaged are smaller than the high-velocity bodies and are associated with the presently active Hengill volcano and the associated fissure swarm. The low-velocity volume located beneath the surface expression of the Hengill volcano is inferred to be a region of partial melt [*Foulger and Toomey*, this issue].

CONCLUSIONS

The simultaneous inversion method of *Thurber* [1981, 1983] was applied to travel time data from earthquakes located within the Hengill-Grensdalur central volcano complex of southwestern Iceland. Within this tectonic regime, which involves rifting and active volcanism, localized crustal structure heterogeneity with anomalous volumes of the order of a few tens of cubic kilometers was expected. Emphasis was thus placed on the fidelity of model parameterization and the resolution of observed structure. In the case of this study, we demonstrate that the density of model parameterization significantly affects the final tomographic image and that a parameterization with good fidelity results in low resolution of individual model parameters. We utilize a spread function that operates on the averaging vector of each model parameter to aid in evaluating model resolution. The spread function is sensitive to nonzero off-diagonal elements of the resolution matrix; thus it is an indicator of the degree of volume averaging for each parameter. Our analysis of resolution and fidelity strongly suggests that high resolution of individual model parameters is a poor measure of the significance of an inversion when the system is under parameterized. An acceptable model parameterization for a given data set should simultaneously consider model fidelity, parameter resolution, and distribution of seismic ray paths. The discussion of model parameterization and analysis of resolution presented here is particularly useful for tomographic studies using parameterized models and a Levenburg-Marquardt damped least squares solution.

Simultaneous inversion of 2409 *P* wave arrival times from 158 earthquakes and two shots, as recorded by a 20-station network, imaged distinct bodies of anomalous velocity. Two high-velocity bodies extend from near the surface to a depth of about 3 km, one of which is associated with the extinct Grensdalur volcano. A third high-velocity anomaly occurs in the depth range 3-4 km but does not extend to the surface. The analysis of resolution shows that the maximum depth extent of this anomaly is poorly resolved. This body lies midway between the Hengill and Grensdalur volcanoes. These anomalies have horizontal dimensions of 3-5 km, and they are interpreted to be solidified magmatic intrusions into the upper crust [*Foulger and Toomey*, this issue]. Relatively low velocities underlay limited portions of the trace of the present accretionary axis, and a low-velocity body is imaged in the roots of the active Hengill volcano. The region of low velocities beneath the Hengill volcano is interpreted to be a volume with partial melt present [*Foulger and Toomey*, this issue].

Acknowledgements. We thank Cliff Thurber for providing important elements of the software used in this analysis and for useful discussions. We also thank Roger Goldsmith and Chan Hilliard for their help with producing Plate 1. Thorough and constructive reviews by Donna Eberhart-Phillips and Bill Ellsworth improved the paper. Collection of the data was funded by the University of Iceland, the National Energy Authority, Iceland and the Reykjavik Municipal District Heating Service. NERC, UK seismological equipment was used. Mike Purdy and Sean Solomon generously supported this study which was undertaken while one of the authors (D.R.T.) was a graduate student in the MIT/WHOI Joint Program in Oceanography. D.R.T. received additional support from the MIT/WHOI Joint Program in Oceanography, the National Science Foundation, under grants EAR-8617967, and from Office of Naval Research, under contract N00014-86-K-0325.

REFERENCES

Aki, K., and W. H. K. Lee, Determination of three-dimensional velocity anomalies under a seismic array using first P arrival times from local earthquakes, 1, A homogeneous initial model, *J. Geophys. Res., 81,* 4381-4399, 1976.

Aki, K., A. Christofferson, and E. S. Husebye, Determination of the three-dimensional seismic structure of the lithosphere, *J. Geophys. Res., 82,* 277-296, 1977.

Angenheister, G., et al., Reykjanes Ridge Seismic Experiment (RRISP 77), *J. Geophys., 47,* 228-238, 1980.

Backus, G. E., and J. F. Gilbert, Numerical application of a formalism for geophysical inverse problems, *Geophys. J. R. Astron. Soc., 13,* 247-276,1967.

Backus, G. E., and F. Gilbert, The resolving power of gross earth data, *Geophys. J. R. Astron. Soc., 16,* 169-205, 1968.

Backus, G. E., and F. Gilbert, Uniqueness in the inversion of inaccurate gross earth data, *Philos. Trans. R. Soc. London, 266,* 123-192, 1970.

Benz, H. M., and R. B. Smith, Simultaneous inversion for lateral velocity variations and hypocenters in the Yellowstone region using earthquake and refraction data, *J. Geophys. Res., 89,* 1208-1220, 1984.

Chou, C. W., and J. R. Booker, A Backus-Gilbert approach to inversion of travel-time data for three-dimensional velocity structure, *Geophys. J.R. Astron. Soc., 59,* 325-344, 1979.

Crosson, R. D., Crustal structure modeling of earthquake data, 1, Simultaneous least squares estimation of hypocenter and velocity parameters, *J. Geophys. Res., 81,* 3036-3046, 1976.

Eberhart-Phillips, D., Three-dimensional velocity structure in northern California Coast Ranges from inversion of local earthquake arrival times, *Bull. Seismol. Soc. Am., 76,* 1025-1052, 1986.

Einarsson, P., and S. Bjornsson, Earthquakes in Iceland, *Joekull, 29,* 37-43, 1979.

Flovenz, O. G., Seismic structure of the Icelandic crust above layer three and the relation between body wave velocity and alteration of the basaltic crust, *J. Geophys., 47,* 211-220, 1980.

Foulger, G. R., Seismological studies at the Hengill geothermal area, SW Iceland, Ph.D. thesis, 313 pp.,Univ. of Durham, England, 1984.

Foulger, G. R., The Hengill triple point, SW Iceland, 1, Tectonic structure and the spatial and temporal distribution of local earthquakes, *J. Geophys. Res., 93,* 13,493-13,506, 1988*a*.

Foulger, G. R., The Hengill triple point, SW Iceland, 2, Anomalous earthquake focal mechanisms and implications for processes within the geothermal reservoir and at accretionary plate boundaries, *J. Geophys. Res., 93,* 13,507-13,523, 1988*b*.

Foulger, G. R., and P. Einarsson, Recent earthquakes in the Hengill-Hellisheidi area in SW-Iceland, *J. Geophys., 47,* 171-175, 1980.

Foulger, G.R., and D.R. Toomey, Structure and evolution of the Hengill-Grensdalur volcanic complex, Iceland: Geology, geophysics, and seismic tomography, *J. Geophys. Res.*, this issue.

Jackson, D. D., Interpretation of inaccurate, insufficient and inconsistent data, *Geophys. J. R. Astron. Soc., 28,* 97-110, 1972.

Jackson, D. D., The use of a priori data to resolve non-uniqueness in linear inversion, *Geophys. J. R. Astron. Soc., 57,* 137-157, 1979.

Klein, F. W., Hypocenter location program HYPOINVERSE, 1, User's guide to versions 1,2,3,4, *U.S. Geol. Surv. Open File Rep., 78-694,* 103 pp., 1978.

Lanczos, C., *Linear Differential Operators*, chapter. 3, Van Nostrand, New York, 1961.

Menke, W., *Geophysical Data Analysis: Discrete Inverse theory*, 260 pp, Academic, San Diego, Calif., 1984.

Palmason, G., Crustal structure of Iceland from explosion seismology, *Visindafelag Isl. Rit., 40,* 187 pp., 1971.

Parker, R. L., The theory of ideal bodies for gravity interpretation, *Geophys. J. R. Astron. Soc., 42,* 315-334, 1975.

Pavlis, G. L., and J. R. Booker, The mixed discrete-continuous inverse problem: Application to the simultaneous determination of earthquake hypocenters and velocity structure, *J. Geophys. Res., 85,* 4801-4810, 1980.

Pavlis, G. L., and J. R. Booker, A study of the importance of nonlinearity in the inversion of earthquake arrival time data for velocity structure, *J. Geophys. Res., 88,* 5047-5055, 1983.

Sabatier, P. C., On geophysical inverse problems and constraints, *J. Geophys., 43,* 115-137, 1977.

Sharp, A. D. L., P. M. Davis, and F. Gray, A low velocity zone beneath Mount Etna and magma storage, *Nature, 287,* 587-591, 1980.

Spencer, C., and D. Gubbins, Travel time inversion for simultaneous earthquake location and velocity structure determination in laterally varying media, *Geophys. J.R. Astron. Soc., 63,* 95-116, 1980.

Tarantola, A., and A. Nercessian, Three-dimensional inversion without blocks, *Geophys. J. R. Astron. Soc., 76,* 299-306, 1984.

Tarantola, A., and B. Valette, Inverse problems = quest for information, *J. Geophys., 50,* 159-170, 1982.

Thurber, C. H., Earth structure and earthquake locations in the Coyote Lake area, central California, Ph.D. thesis, 332 pp., Mass. Inst. of Technol., Cambridge, 1981.

Thurber, C. H., Earthquake locations and three-dimensional crustal structure in the Coyote Lake area, central California, *J. Geophys. Res., 88,* 8226-8236, 1983.

Thurber, C. H., and K. Aki, Three-dimensional seismic imaging, *Annu Rev. Earth Planet. Sci., 15,* 115-139, 1987.

Thurber, C. H., and W. L. Ellsworth, Rapid solution of ray tracing problems in heterogeneous media, *Bull. Seismol. Soc. Am., 70,* 1137-1148, 1980.

Wiggins, R. A., The general linear inverse problem: Implication of surface waves and free oscillations for earth structure, *Rev. Geophys., 10,* 251-285, 1972.

G.R. Foulger, Department of Geological Sciences, University of Durham, Science Laboratories, South Road, Durham DH1 3LE, England.

D.R. Toomey, Department of Earth, Atmospheric, and Planetary Sciences, Room 54-512, Massachusetts Institute of Technology, Cambridge, MA 02139.

(Received January 3, 1989;
revised May 19, 1989;
accepted May 20, 1989)